AUT Journal of Electrical Engineering

AUT J. Elec. Eng., 54 (Special Issue 2) (2022) 409-420
DOI: 10.22060/eej.2022.21186.5463

Diagnosing Cancerous Tumor Using Photoacoustic Imaging and Thermoacoustic Tomography with Electric Excitation Techniques-A Numerical Approach for Comparison

M. Ahangar Darband[1], E. Najafi Aghdam[1*], A. Gharibi[2]

[1] Electronic Engineering, Department of Electrical Engineering, Sahand University of Technology, Tabriz, Iran
[2]Electronic engineering, Institute of Modern Physics, Shanxi Normal University, Linfen, P. R. China

ABSTRACT: A numerical study and simulation of cancerous tumor detection using the Photoacoustic (PA) phenomenon and Thermoacoustic Tomography with Electric Excitation (TATE) are presented. This report was in a small dimension of mimic breast tissue. Moreover, the different layers of the breast were considered. The optical, thermal, elastic, electric, and acoustic characteristics of different layers of the breast tissue and tumor at a radiated laser wavelength (800 nm), and electric voltage pulse were accurately calculated or obtained from reliable sources to calculate accurately and realistically. Furthermore, the amount and power of voltage and laser have been selected as the minimum allowable values to accurately compare the two methods. Therefore, it was possible to rely on the values and characteristics of the resulting data in comparing the accuracy and clarification of the two methods. A single suitable platform for simulating, which is commercially available Finite Element software (COMSOL®), has been selected. By using this platform, we were able to simulate these two methods from stimulation to propagation continuously. Finally, by studying the data matrix of the two simulations, we can demonstrate the maximum difference of stress in and out of tumor in the two methods is about 0.1 Pa higher in PAT relative to the TATE. It means PAT is more accurate than TATE, and the combination of these two methods can be ideal for the accurate and complete study of cancerous tumors.

Review History:

Received: Mar. 05, 2022
Revised: May, 26, 2022
Accepted: Jun. 06, 2022
Available Online: Dec. 01, 2022

Keywords:

Photo-Acoustic Imaging (PAI)
Thermoacoustic (TA)
Thermoacoustic Tomography with Electric Excitation (TATE)
Breast Cancer
Early Diagnosis.

1- Introduction

Breast cancer is one of the most common forms of cancer among females, but it is less common among men. Breast cancer typically has no symptoms when the tumor is small and can be easily treated, thus screening is vital for early detection [1]. There are various methods for attentively examining breast tissue to identify cancerous tumors. However, a low-risk, non-invasive, accessible, accurate, and low costs method that can detect cancerous tumors in the early stages of the disease is a priority. Among the available imaging modalities for tissue tomography, our focus is on thermo/opto-acoustic imaging, and finding a more accessible and accurate approach to the early detection of breast cancer. The Photoacoustic (PA) approach combines pure optical and pure acoustic imaging methods and takes the best of both. The main limitation of the pure optical imaging modalities is the scattering of light in the environment which lowers the spatial resolution in deep tissue imaging [2]. In pure acoustic imaging, the contrast of the image is determined by the mechanical and elastic properties of the living tissue. Therefore, the contrast of the images may not be suitable for the early detection of a cancerous tumor [3], [4]. Photoacoustic Imaging (PAI) has become an attractive, low-risk, and non-invasive tool in imaging biological tissues using non- ionized short laser pulse absorption and receiving PA signals. The PAI is based on the PA phenomenon discovered in 1880 by Alexander Graham Bell. It refers to the generation of acoustic waves by the absorption of Electromagnetic energies, such as a laser. The acoustic wave is produced due to the thermoelastic expansion induced by a slight temperature rise, typically in the millikelvin range, as a result of the energy deposition inside the biological tissue through the absorption of the incident Electromagnetic (EM) energy. The excited PA signal is locally determined by the EM absorption and scattering properties, the thermal properties (including the thermal diffusivity and thermal expansion coefficient), and the elastic properties of the sample [5], [6]. We can use this phenomenon to diagnose cancerous tumors. PAI is one of our choices in this review. Electrical Impedance Tomography (EIT) has the ability to image the electrical parameters of tissue through current injection and the measurements of surface voltage [7] However, EIT has a low spatial resolution. Versus Thermoacoustic Tomography with Electric Excitation (TATE) is a new imaging method and has attracted much more attention recently because it's based on the hybrid imaging technology, and has high contrast and resolution, similar to PAI [8].

In TATE, using two surface electrodes, a short power electric pulse is applied to the tissue, and the current density will be generated in the tissue through the electrodes. This produces Joule heat in the tissue, which in turn generates the ultrasonic signal by Thermoacoustic effect. The ultrasonic signal

*Corresponding author's email: najafiaghdam@sut.ac.ir

can be collected by the transducer. Finally, the Joule heat distribution can be calculated from the collected ultrasonic signal. The Joule heat distribution map is closely related to the conductivity distribution. Due to the conductivity differences in different materials, we are able to diagnose a tumor in the tissue. With this brief introduction, we tried to study the ability and accuracy of these two methods in early detecting of breast cancerous tumors in this article. To have a risk-free environment and insight into dynamics, visualization, increasing accuracy, handling uncertainty, and saving money and time, we start with simulation. There are two methods for simulating different blocks of the PA phenomenon. The first case is using the Monte Carlo model of steady-state light transport in Multi-Layered Tissue (MCML) in determining the amount of light absorption in the studied tissue [9, 10]. Afterwards, to simulate the time-domain PA propagating in one, two, and three dimensions at a homogeneous/heterogeneous medium, we should import absorption data matrix in the K-wave MATLAB toolbox [11]. This simulation process is incoherent.

However, MCML is very time-consuming [12, 13]. In the case of MCML and K-wave toolbox, we cannot maneuver on the actual shape, size and geometry of the tissue [14]. Another method is the Finite Element Method (FEM). Obviously, the FEM method is much more efficient and accurate than the MC method [15]. Thus, we switch to a single platform to carefully model and solve the problems expressed. Our choice is commercially available Finite Element software (COMSOL) as a single platform for simulating Photoacoustic Imaging (PAI) [16]. COMSOL was also selected for accurate and error-free comparisons as TATE simulation platform. Here, we want to simulate PAI and TATE and study their difference. Our mimic tissue is in small size with different layers of the breast.

2- Method

In this section, we will briefly describe the governing equations of PAI and TATE phenomenon. Afterwards, the simulation processes are discussed. Different modules of COMSOL software, Finite Element modeling, and their necessary parameters have also been listed. The remaining sections will be about the study of reports resulting from simulation.

2- 1- A brief Description of the Mathematical Equations

2- 1- 1- PAI Mathematical Model

Using linear fluid dynamics equations, a pair of coupled differential equations for temperature and pressure can be developed. According to Morse and Ingard, changes in temperature (T) and pressure (p) from their ambient values can be expressed as follows [4], [17]:

$$\frac{\partial}{\partial t}\left(T-\frac{\gamma-1}{\gamma\alpha}p\right)=\frac{k}{\rho C_p}\nabla^2 T+\frac{H}{\rho C_p} \quad (1)$$

and

$$\left[\nabla^2-\frac{\gamma}{v_s^2}\frac{\partial^2}{\partial t^2}\right]p=-\frac{\alpha\gamma}{v_s^2}\frac{\partial^2}{\partial t^2}T \quad (2)$$

Where γ is an specific heat ratio, $\alpha\left(\text{pressure expansion coefficient}\right)=\left(\frac{\partial p\left(\text{pressure}\right)}{\partial T\ \left(\text{temperature}\right)}\right)_{V\ (\text{volume})}$, k is the thermal conductivity, ρ is the ambient density, v_s is the sound speed, t is the time, and H is the energy per unit volume and time deposited by the optical radiation beam [4].

The above equations did not include the effects of viscosity or energy relaxation. Assuming that γ=1, which for most fluids is a common and acceptable assumption, and assuming heat conductivity is set to zero (∇T=0), then equations 1 and 2 reduce to an equation for heat diffusion and a wave equation relating pressure to the speed of sound:

$$\left[\nabla^2-\frac{1}{v_s^2}\frac{\partial^2}{\partial t^2}\right]p=-\frac{\beta}{C_p}\frac{\partial H}{\partial t}$$

$$\beta=(1/V)(\partial V/\partial T)_p \quad (3)$$

$$\alpha=\rho\beta v_s^2/\gamma$$

V is the volume, and T is the temperature [18].

To improve the optimal feature of the PA signal, the duration of pulsed laser light radiation, τ, must be a few nanoseconds to include the following two conditions: 1) thermal confinement, which represents the neglect of thermal diffusion during laser light irradiation [19].

$$\tau<\tau_{th}=\frac{{d_c}^2}{4D_T} \quad (4)$$

τ_{th} : thermal confinement threshold
D_T : thermal diffusivity
d_c : desired special resolution.

2) Stress confinement means neglecting the volume expansion of the absorber during laser light irradiation.

$$\tau<\tau_{st}=\frac{d_c}{V_S} \quad (5)$$

τ_{st} : the stress confinement threshold
V_S : speed of sound

Under both conditions, irradiation time can be treated as a delta function [19].

Hence, we would be able to rewrite equation (3) in the form of:

$$\left[\nabla^2-\frac{1}{v_s^2}\frac{\partial^2}{\partial t^2}\right]p(r.t)=-\frac{p_0}{v_s^2}\frac{\partial\delta(t)}{\partial t} \quad (6)$$

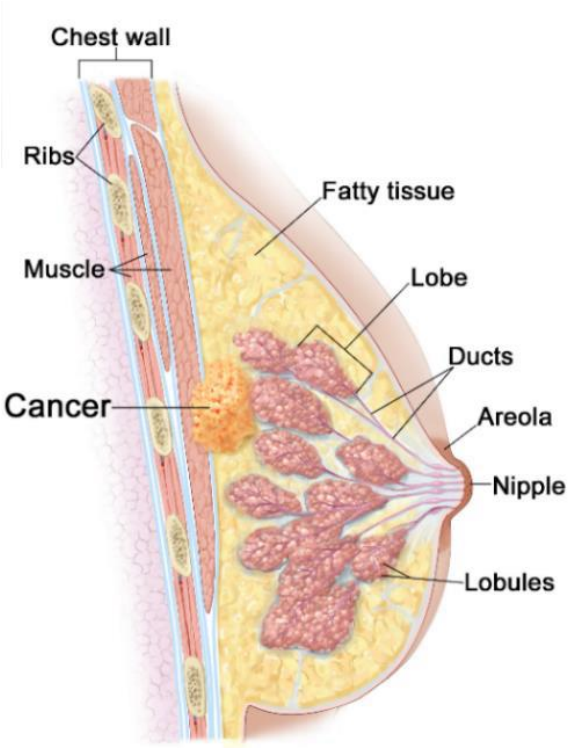

Figure 1. Cross-sectional image of the breast tissue including tumor inside [21].

The acoustic wave p(r,t) at position r and time t, prompted by initial source, $p_0(r)=\Gamma(r)A_e(r)$ where $A_e(r)$, is a spatial Electromagnetic (EM) absorption function, and $\Gamma(r)=v_s^2\beta/C_p$ is the Grüneisen parameter [18]. In this equation, by studying the ultrasonic wave, its propagation, and intensity, we can realize the structure of the sample and thus the tissue imaging.

2- 1- 2- TATE Mathematical Model

In TATE, the source of stimulation is a short voltage pulse. If thermal confinement and stress confinement conditions are met, the generated ultrasonic wave can be efficient for imaging. By using Joule's law, the Joule heat Qin is [8]:

$$Q_{in} = \int_0^{t_{th}} I(t) \times I(t) \times R dt \tag{7}$$

t_{th} is the duration time, I(t) is the current, and R is the resistance of the tissue.

In general:

$$I(t) = \int_0^{S_I} J.dS \tag{8}$$

$$R = \int_0^{V_I} \frac{1}{\sigma} \frac{dl}{dS} \tag{9}$$

In above equations, J is the current density distribution of the tissue, σ is the conductivity, and S_I is the acreage of cross section. Therefore, we can rewrite Q_{in} as:

$$Q_{in} = \int_0^{t_{th}} \int_0^{V_I} \frac{1}{\sigma} J.JdVdt \tag{10}$$

According the PAI mathematical model, Eq. 6, we can rewrite TATE final equation as:

$$\left[\nabla^2 - \frac{1}{v_s^2}\frac{\partial^2}{\partial t^2}\right] p(r.t) = -\frac{\beta}{C_p}\frac{\partial(\frac{d((1-\theta)Q_{in})}{dV})}{\partial t} \tag{11}$$

In practice, θ is related to the variation of heat capacity. Eq. 11 is the main equation of TATE. The ultrasonic signal p is the measurement signal of TATE, which we are able to map the Joule heat distribution by reconstructing the p signal.

2- 2- Finite Element Method (FEM) & Comsol Multiphysics Model

2- 2- 1- Breast Tissue Anatomy and Cancer Location

A cross-sectional of the normal breast consist of the Chest wall, Pectoralis muscles, Lobules, Nipple, Areola, Milk duct, Fatty tissues and the Skin [20]. A cross-section image of the breast tissue with a tumor inside is shown in Fig.1. Most of the initial development of cancer occurs inside the glandular tissue. Breast cancer can be in either lobes or ducts [1]. To

simplify this study, only the layers of breast tissue that are most involved with cancerous tumors are considered.

3- Mimic Breast Tissue Model in Simulation

In our simulation model, different parts of the breast tissue are separated to discriminate the distinct characteristics of each part required in the steps of acoustic wave propagation. A 2D circular layer of breast tissue at block workplace of water in 130mm depth, width and thickness of 4 mm has been modeled with different layers. PAI and TATE geometry are shown in Fig. 2. Circular adipose, gland and tumor in diameter, 40mm, 20mm and 2mm were considered, respectively. The entire mimic tissue is enclosed inside a block of water, except in the top which is exposed to the air. For a better conception of the PAI and TATE process and the procedure of the simulations, a schematic flowchart is illustrated in Fig. 3

4- TATE Simulation Model

For this part of the simulation in COMSOL Multiphysics, we used the "Joule heat" module in order to convert the applied voltage into heat in the mimic tissue. The excitation voltage applied to the tissue through the two electrodes, shown in Fig.2) a, is $U(t)=U\exp\left(\frac{-(t-b)^2}{2c^2}\right)$, with $b=5\times10^{-7}$ and $c=1\times10^{-7}$. Afterwards, "Solid Mechanics" module converts the heat into stress. Propagation of acoustic wave could be modeled by using "Pressure Acoustics, Transient" module, Perfectly Matched Layer (PML) was used as boundary condition to minimize reflections. The two final steps are common in the two simulations.

4- 1- PAI Simulation Model

"Coefficient Form PDE" module is used for computing the laser effect on different parts of the mimic breast tissue. Here, we modeled radiated laser source as Gaussian pulse in a 800 nm wavelength, with the power of $W_p=8\,\mathrm{mJ/cm^2}$, pulse duration of $\tau_p=10\,\mathrm{ns}$, and $\tau_{center}=30\,\mathrm{ns}$. The diffusion equation of the fluence rate φ is represented by:

$$\nabla.(-D\nabla\emptyset)+a=f \tag{12}$$

D is the diffusion coefficient
a is the absorption coefficient
f is the function of laser pulse.

Laser pulse should be radiated in homogenized mode on tissue. The Boundary conditions were based on Snell's Law [13]. In the following, we are able to export the laser pulse fluence as Heat Flux in the "Bioheat Transfer" module, and convert it to heat. The rest of the modules will be similar to the TATE simulation.

4- 2- All Required Properties of Each Layer of Breast Tissue

The optical properties of the tumor and glandular tissue depend on the assumed magnitude of absorbers that have a dramatic effect on the given wavelength. Once the optical properties are obtained at each wavelength, we can calculate the absorption coefficient of light ($\mu_a\left(\mathrm{cm^{-1}}\right)$) of an absorber by using one of these equations [22]:

$$\mu_a=-\frac{1}{T}\frac{\partial T}{\partial L} \tag{13}$$

$$T=e^{-\mu_a L}=10^{-\varepsilon CL}=e^{-4\pi n'' L/\lambda} \tag{14}$$

T (dimensionless) is a transmitted or surviving fraction of the incident light after an incremental pathlength ∂L (cm), n'' is the imaginary refractive index of the medium, ε is the extinction coefficient ($cm^{-1}\,M^{-1}$), and C (M) is the concentration of chromophore. The absorption coefficient of a tissue is the sum of all main absorbers:

$$\mu_a=\ln(10)\sum_i C_i\varepsilon_i \tag{15}$$

Additionally, the reduced scattering (or transport scattering) coefficient of light, $\mu_s'\left(\mathrm{mm^{-1}}\right)$, and the spectrum of tissue has been shown to fit well to an empirical approximation to Mie scattering theory given by [23]:

$$\mu_s'=a\lambda^{-b} \tag{16}$$

In this equation, (a) and (b) are the scatter amplitude and the scatter power at any wavelength in ì m , respectively.

The percentage of absorbent ingredients of tumor, glandular tissue, and adipose of breast is based on [23]. The spectral characteristics of HHb, HbO_2, and water at 800 nm are taken from references25 ,24]]. The optical parameters of breast tissue sections and tumor used in PAI the accurate electric properties of breast layers and tumor in TATE have been entered in Table 1.

5- Results and Discussion

Using the Finite Element (FE)-based simulation models, light propagation and Joule heating, absorption, conversion to heat, PA and TATE wave formation from the target (tumor), and its propagation in mimic breast tissue were successfully simulated. Finally, comparative results of the two simulation methods concerning the amplitude of the acoustic were studied in detail. The electric potential profile in the TATE simulation is shown in Fig. 4.

In the TATE simulation, increasing the temperature of mimic tissue and tumor happened, but more increment takes place in tumor. Fig. 5. a) shows the profile of stress which is caused from Joule heat. The stress distribution of tumors has been imaged clearly. TATE has the potential to image the tumors with acceptable contrast and resolution. Results of PAI simulation shows the profile of stress in Solid Mechanics module, and is clearer and the amplitude of pressure is a little higher than the TATE simulation,

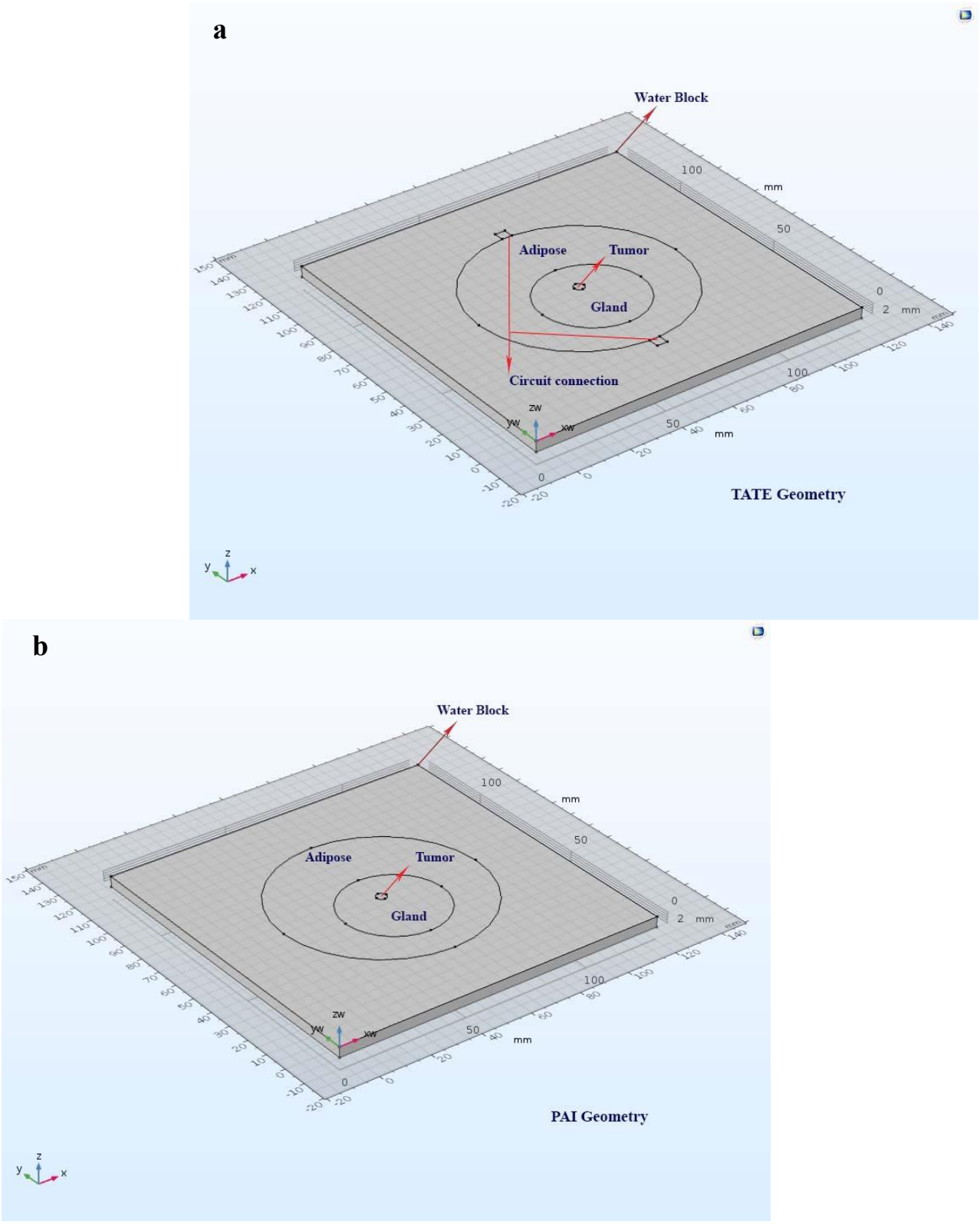

Fig. 2. The schematic structure of the simulation in COMSOL, a) TATE geometry, b) PAI geometry.

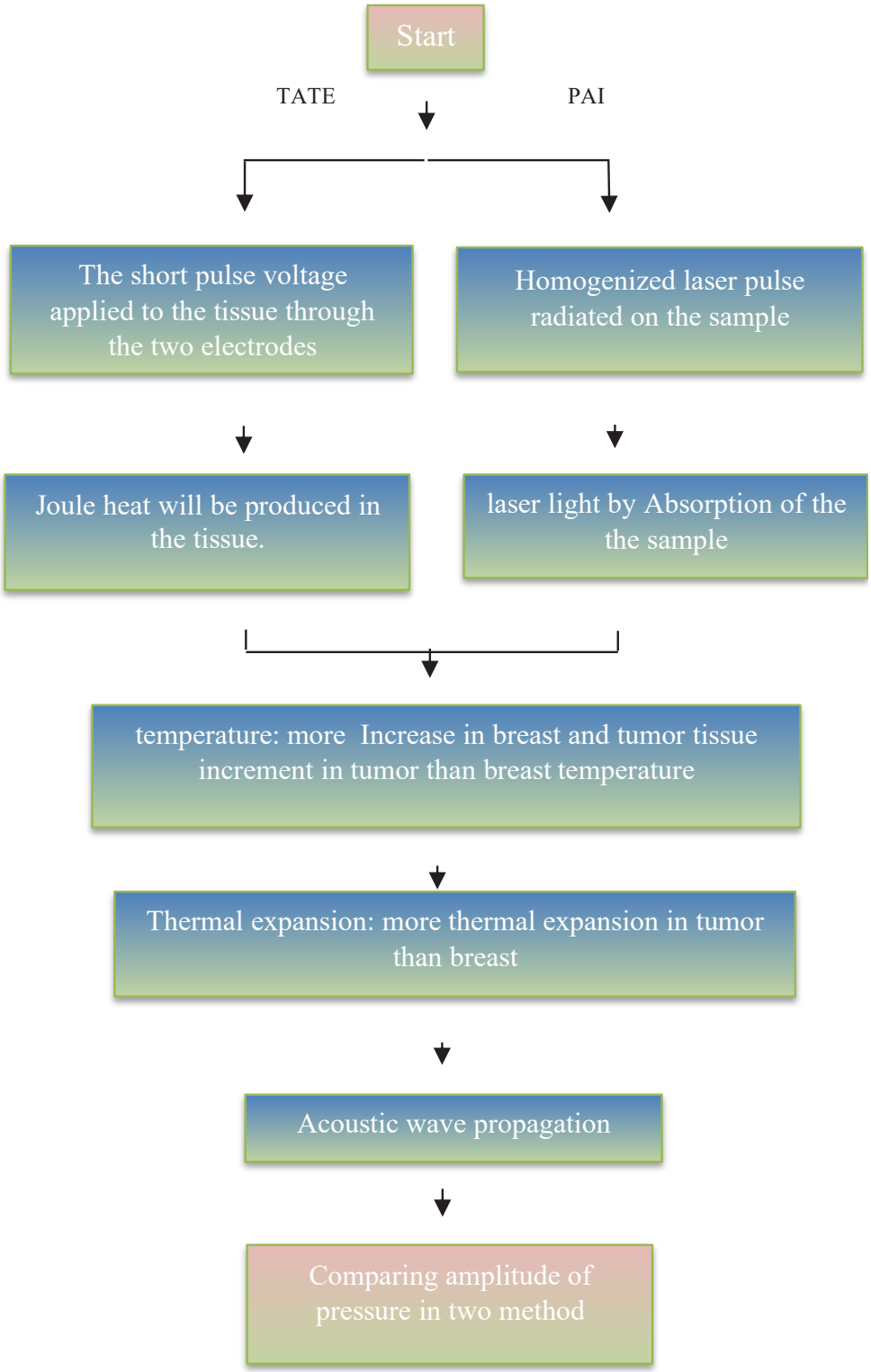

Fig. 3. Flowchart description of the procedure of simulations.

Table 1. Thermal, acoustic and optical parameters of breast tissue and tumor at 800 nm [26] [27] [28] [29] [30] [27, 31, 32]

Parameter	Tumor	Adipose	Glandular	Water
Density, ρ (kg/m^3)	1050	930	1050	994
Poisson's Ratio	0.495	0.49	0.49	0.4995
Young's Modulus (Pa)	106E3	18E3	50E3	Bulk Modulus=2.1790576GPa
Refractive Index	1.4	1.455	1.4	1.329
Thermal conductivity, k (W/m.k)	0.54	0.21	0.48	0.60
Specific heat capacity, C (J/kg.k)	3852	2770	3770	4178
Coefficient of thermal expansion, β (K^{-1})	6.5E-5	3E-5	4.5E-5	~24E-5
Speed of sound, C_s (m/s)	1540	1440.2	1505.0	1482.3
μ_a at 800 nm (mm^{-1})	0.00302	0.00193	0.00436	0.00196
μ_s'at 800 nm (mm^{-1})	0.625	1.52	1.12	0.0000402

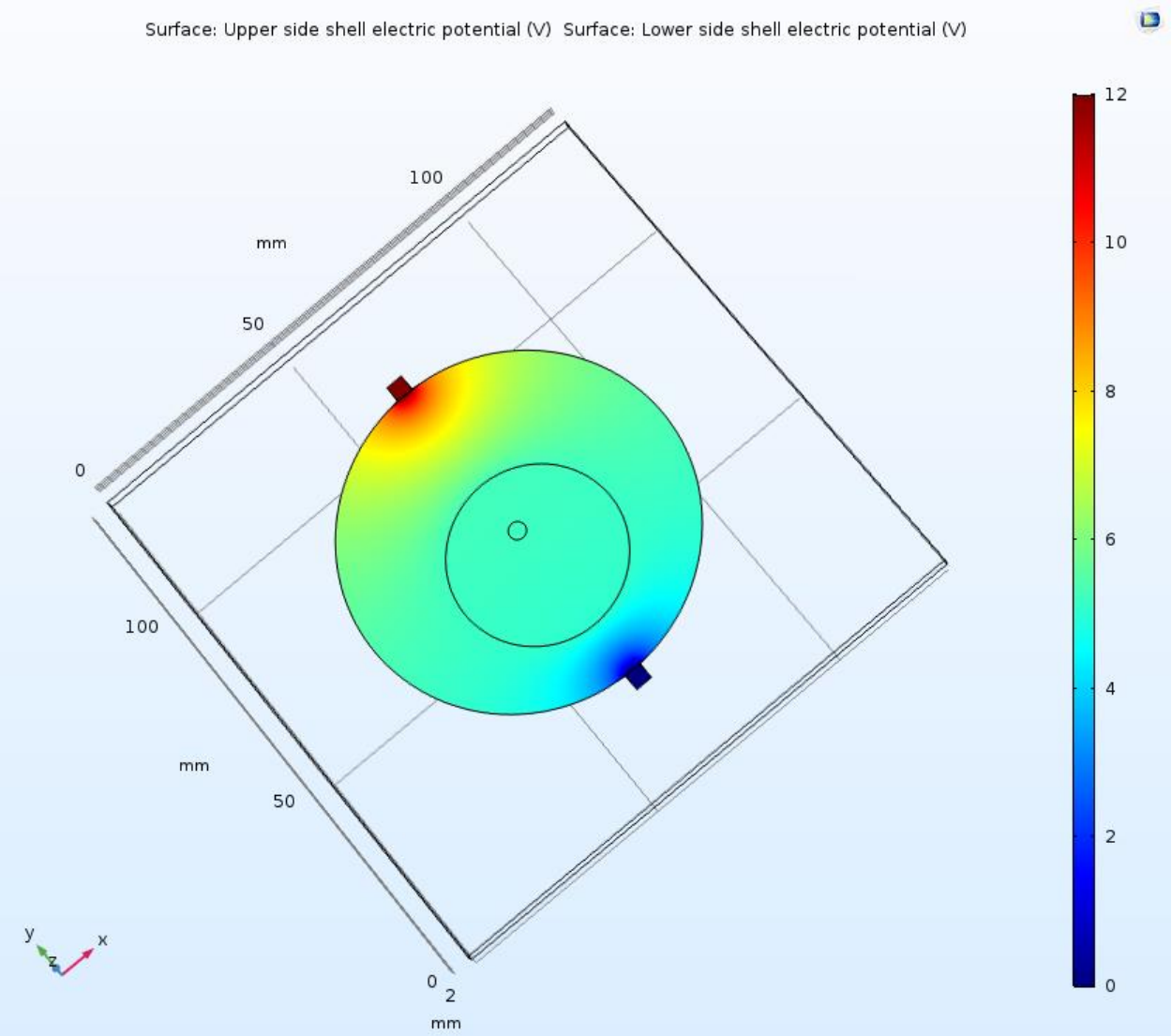

Fig. 4. Electric Potential profile at the primitive time of simulation in TATE simulation

Finally, by studying the data matrix of the two simulations exported from COMSOL, we compare the maximum difference of stress in and out of the tumor. As seen in Fig. 6, this difference is about 0.1 Pa higher in PAT relative to the TATE. With respect to this simulation, which has been preformed in small dimensions, it seems that this difference will also exist in real dimensions and is significant. According to the study in references [33, 34], it seems that the distinction between optical properties is more accurate and powerful than the electrical properties of breast tissue and tumors.

All our studies in COMSOL are in an Stationary Solver form. We have a limitation in the value of current distribution in Joule heat for facing by biological sample, thus controlling the current distribution with a safe level is necessary. In PAI, Red and Near-InfraRed (NIR) wavelengths are usually preferred because, in this wavelength range, the optical attenuation of biological tissue is on its lowest level. HbO_2, HHb, and water are assumed to be the main absorbers in this study. In particular, a wavelength of around 800 nm is the isosbestic point of the molar extinction spectra of HbO_2 and HHb [18]. This wavelength is non-Ionized and safe. Additionally, the maximum permissible pulse energy and the maximum permissible pulse repetition rate are governed by the "American National Standard for the Safe Use of Lasers (ANSI)" laser safety standards [25]. In order to accurately compare the two methods, the amount and power of voltage and laser have been selected as the minimum allowable values. Using laser pulse in PAI causes this method to be more expensive than TATE. However, it seems that the combination of these two methods in the careful study of breast tissue for the early diagnosis of cancerous tumors can be accurate and appropriate [34].

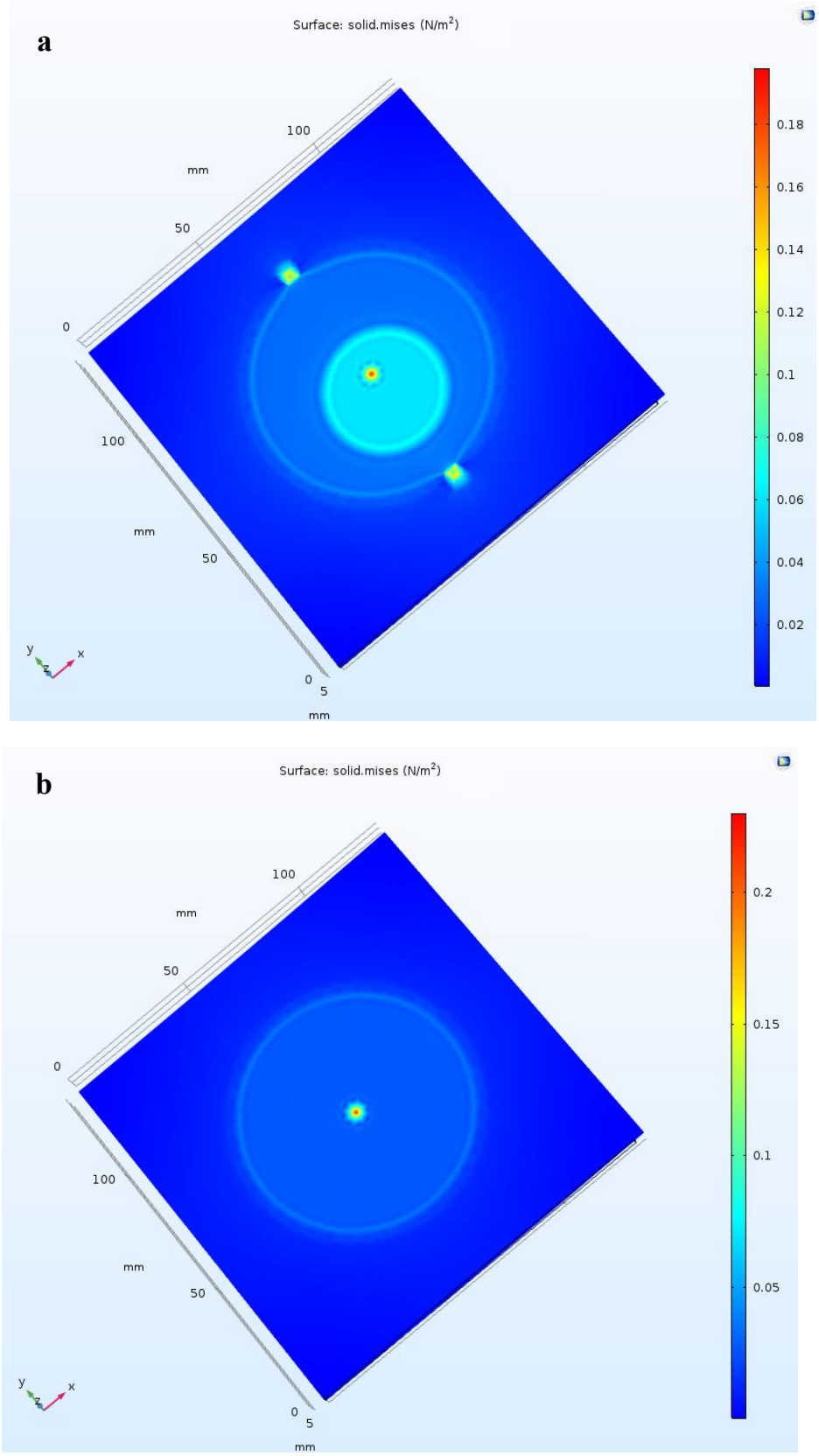

Fig. 5. stress profile in a) TATE simulation and, b) in PAI simulation.

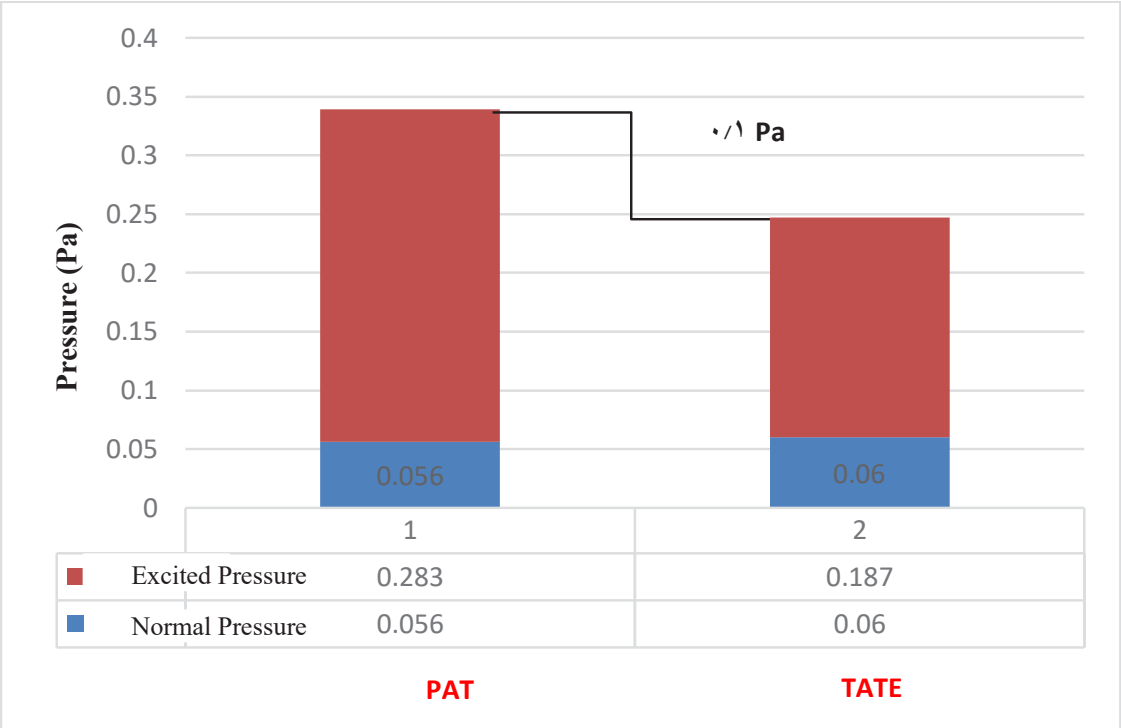

Fig. 6. Numerical comparison of two methods in tumor edge detection

6- Conclusion

In this study, simulation of PAI and TATE in diagnosing cancerous tumor in mimic breast tissue by considering different constituent layers of the breast and, with a cancerous tumor, has been modeled. Attempts were also made to consider the different layers that make up the breast tissue and enter all the required specifications in the simulation in a complete and accurate manner. The goal was to compare the two methods of diagnosing tumors, and find their advantages and disadvantages. In both methods, due to the electrical/optical, thermal, elastic, and acoustic characteristics of different layers of mimic breast tissue and tumor, the tumor shows a greater difference in propagating acoustic waves compared to other layers. This difference helps us to diagnose cancerous tumors. The results show that the acoustic pressure magnitude and contrast of tumor diagnosing will be higher in PAI. It is quite clear that PAI and TATE methods can be suitable approaches to diagnosing cancerous tumors. However, due to the capability of the PA phenomenon and its higher optical contrast, it was able to detect tumors better and clearer than TATE. It seems that the combination of these two methods can be complementary and provide more accurate results.

Data Availability

The data that support the findings of this study are available from the corresponding author upon reasonable request.

References

[1] Soc, A.C.S.J.A.C., Breast cancer facts & figures 2019–2020. 2019: p. 1-44.

[2] Wang, L.V.J.I.J.o.S.T.i.Q.E., Tutorial on Photoacoustic microscopy and computed tomography. 2008. 14(1): p. 171-179.

[3] Wang, L.V.J.D.m., Ultrasound-mediated biophotonic imaging: a review of acousto-optical tomography and photo-acoustic tomography. 2004. 19(2-3): p. 123-138.

[4] Mozaffarzadeh, M., et al., Double-stage delay multiply and sum beamforming algorithm: Application to linear-array Photoacoustic Imaging. 2017. 65(1): p. 31-42.

[5] Mozaffarzadeh, M., et al., Linear-array Photoacoustic Imaging using minimum variance-based delay multiply and sum adaptive beamforming algorithm. 2018. 23(2): p. 026002.

[6] Xu, M. and L.V.J.R.o.s.i. Wang, Photoacoustic Imaging in biomedicine. 2006. 77(4): p. 041101.

[7] Bera, T.K., J. Nagaraju, and G.J.J.o.V. Lubineau, Electrical impedance spectroscopy (EIS)-based evaluation of biological tissue phantoms to study multifrequency Electrical Impedance Tomography (Mf-EIT) systems. 2016. 19(4): p. 691-713.

[8] Song, J., et al., Three-dimensional model of Thermoacoustic Tomography with Electric Excitation.

2018. 124(16): p. 164902.

[9] Wang, L., et al., MCML—Monte Carlo modeling of light transport in Multi-Layered Tissue s. 1995. 47(2): p. 131-146.

[10] Wang, L. and S.L.J.T.U.o.T. Jacques, MD Anderson Cancer Center, Houston, Monte Carlo modeling of light transport in Multi-Layered Tissue s in standard C. 1992. 4(11).

[11] Treeby, B.E. and B.T.J.J.o.b.o. Cox, k-Wave: MATLAB toolbox for the simulation and reconstruction of Photoacoustic wave fields. 2010. 15(2): p. 021314.

[12] Cassidy, J., et al., High-performance, robustly verified Monte Carlo simulation with FullMonte. 2018. 23(8): p. 085001.

[13] Wang, Z., S. Ha, and K. Kim. Evaluation of finite-element-based simulation model of Photoacoustic s in biological tissues. in Medical Imaging 2012: Ultrasonic Imaging, Tomography, and Therapy. 2012. International Society for Optics and Photonics.

[14] Akhlaghi, N., et al., Multidomain computational modeling of Photoacoustic Imaging: verification, validation, and image quality prediction. 2019. 24(12): p. 121910.

[15] Xu, Y. and Q. Zhu. Comparison of Finite Element and Monte Carlo simulations for inhomogeneous advanced breast cancer imaging. in Excerpt from the Proc. of the COMSOL Conf. Boston. 2010.

[16] Multiphysics, C., 3.4, COMSOL AB, Stockholm, Sweden.

[17] Omidi, P., et al., A novel dictionary-based image reconstruction for Photoacoustic computed tomography. 2018. 8(9): p. 1570.

[18] Wang, L.V., Photoacoustic Imaging and spectroscopy. 2017: CRC press.

[19] Li, C., L.V.J.P.i.M. Wang, and Biology, Photoacoustic tomography and sensing in biomedicine. 2009. 54(19): p. R59.

[20] Lynch, P.J.J.C.f.A.I.M., illustrator; C. Carl Jaffe; MD; cardiologist Yale University Center for Advanced Instructional Media Medical Illustrations by Patrick Lynch, generated for multimedia teaching projects by the Yale University School of Medicine. 1987. 2000.

[21] Paruch, M.J.M., Mathematical modeling of breast tumor destruction using fast heating during radiofrequency ablation. 2019. 13(1): p. 136.

[22] Jacques, S.L.J.P.i.M. and Biology, Optical properties of biological tissues: a review. 2013. 58(11): p. R37.

[23] Dehghani, H., et al., Near infrared optical tomography using NIRFAST: Algorithm for numerical model and image reconstruction. 2009. 25(6): p. 711-732.

[24] Hale, G.M. and M.R.J.A.o. Querry, Optical constants of water in the 200-nm to 200-μm wavelength region. 1973. 12(3): p. 555-563.

[25] Prahl, S., Assorted Spectra. 2017.

[26] Foundation, I.I., Tissue Properties Database V4. 0. 2011.

[27] Soltani, M., et al., Breast cancer diagnosis with a microwave Thermoacoustic imaging technique—a numerical approach. 2019. 57(7): p. 1497-1513.

[28] Grimal, Q., S. Naïli, and A.J.J.o.b. Watzky, A high-frequency lung injury mechanism in blunt thoracic impact. 2005. 38(6): p. 1247-1254.

[29] Zhutovsky, S. and K. Kovler, Evaluation of the thermal expansion coefficient using non-destructive testing, in CONCREEP 10. 2015. p. 1137-1146.

[30] Li, C., et al., In vivo breast sound-speed imaging with ultrasound tomography. 2009. 35(10): p. 1615-1628.

[31] Bhatti, S.N. and M.J.M.P. Sridhar-Keralapura, A novel breast software phantom for biomechanical modeling of elastography. 2012. 39(4): p. 1748-1768.

[32] Gefen, A., B.J.T. Dilmoney, and H. Care, Mechanics of the normal woman's breast. 2007. 15(4): p. 259-271.

[33] Pal, U.M., et al., Thermo-optic measurements and their inter-dependencies for delineating cancerous breast biopsy tissue from adjacent normal. 2021. 14(8): p. e202100041.

[34] Shokoufi, M., Multi-modality breast cancer assessment tools using diffuse optical and electrical impedance spectroscopy. 2016, Applied Sciences: School of Mechatronic Systems Engineering.

HOW TO CITE THIS ARTICLE

M. Ahangar Darband, E. Najafi Aghdam, A. Gharibi, Diagnosing Cancerous Tumor Using Photoacoustic Imaging and Thermoacoustic Tomography with Electric Excitation Techniques—A Numerical Approach for Comparison, AUT J. Elec. Eng., 54(Special Issue 2) (2022) 409-420.

DOI: 10.22060/eej.2022.21186.5463